Hindawi
Wireless Communications and Mobile Computing
Volume 2022, Article ID 4481416, 9 pages
https://doi.org/10.1155/2022/4481416

Research Article

Few-Shot Specific Emitter Identification Based on Variational Mode Decomposition and Meta-Learning

CunXiang Xie[1], **LiMin Zhang**[1] and **ZhaoGen Zhong**[2]

[1]*Department of Information Fusion, Naval Aviation University, Yantai 264001, China*
[2]*The School of Aviation Basis, Naval Aviation University, Yantai 264001, China*

Correspondence should be addressed to ZhaoGen Zhong; zhongzhaogen@163.com

Received 24 May 2022; Revised 30 June 2022; Accepted 2 July 2022; Published 14 July 2022

Academic Editor: Xingwang Li

Recently, deep learning has become the mainstream solution to solve specific emitter identification (SEI) problems. However, because large amounts of labeled signal samples cannot be obtained in noncooperative scenarios, the performance of deep learning-based data-driven methods for SEI was limited. As a result, a novel SEI method targeted on few-shot was proposed in this study. First, the received signal was preprocessed based on variational mode decomposition and the Hilbert analysis to obtain the Hilbert time-frequency spectrum. Subsequently, a classification neural network model was built and trained with a small number of Hilbert time-frequency spectrum samples through meta-learning. This model could identify specific emitters with limited training samples. The experimental results showed that this method accomplishes network training with as few as 80 training samples while obtaining a good level of generalization and effectively identifying different emitter individuals. In addition, this method exhibits a strong robustness to noise by maintaining an identification accuracy of more than 80% in channels with low signal-to-noise ratios. Finally, the proposed method demonstrated better identification performances than other existing methods with its capability to effectively solve SEI problems in the few-shot scenario.

1. Introduction

Specific emitter identification (SEI) refers to a technology that correlates a received signal to its emitting source, only utilizing certain external features of the signal [1–3]. Such external features, often referred to as radiofrequency fingerprints (RFFs) of the specific emitting source, are generated by the nonlinear characteristics of the hardware inside the emitter. They are unique, independent of the signal content, and consistent in different signals from the same emitter. However, signals emitted from different emitters exhibit distinct features, i.e., they are distinguishable RFFs, even if the emitter devices are from the same manufacturer, of the same model, or even of the same batch [4–6].

SEI is a crucial technology for cognitive radio [7, 8]. Dynamic spectrum access (DSA), an effective method of improving spectrum utilization, allows cognitive radio networks to use the current spectral resources more efficiently [9–12]. Moreover, to solve the problem of mutual interferences in DSA networks, identity authentication has usually been used to ensure the security of wireless communication systems. Through SEI, subtle features of the wireless radio signals can be determined with the help of signal processing techniques. Subsequently, together with the critical system, a hardware–software dual authentication system can be established to improve the security performance of the wireless system significantly.

In contrast, wireless radio technologies have been widely used across various industries. Mutual interferences between radio services and spectrum congestions must be prevented and avoided to meet the wireless industry's increasing demand for radio spectrums. For this purpose, legitimate radio stations must be monitored for strict compliance with the designated working parameters. Moreover, pirate radios must be tracked down. By applying SEI techniques to the captured signals in the radio monitoring equipment, it becomes possible to distinguish between the legitimate and pirate radio stations by analyzing the working parameters within the frequency bands allocated to them and extracting their hardware features. In this manner, regulating the usage of spectrum resources can

be achieved. Moreover, it enhances the radio equipment's ability to distinguish users of different nature, as well as in the detection of unknown interference signals.

In recent years, extensive research on SEI has been conducted. Padilla et al. [13] proposed a method to extract RFFs which utilizes the spectrum information of signal preambles, with which several Wi-Fi devices have been successfully identified. Yuan et al. [14] designed an algorithm that can extract 13 features of the time-frequency power spectrum of RF signals to construct a feature vector for SEI. Although redundancies have been found in the extracted features, the represented information has still been considered insufficient, limiting the identification performance. Zhang et al. [15] extracted the energy entropy, first moment, and second moment of the time-frequency power spectrum as RFFs. However, the time-frequency power spectrum has not been partitioned, implying a lack of consideration of the power distribution across the spectrum, the impact of which on the identification performance can hardly be neglected. Satija et al. [16] decomposed the received RF signals into finite modal components through variational mode decomposition (VMD). With the VMD entropy and cumulant constructed as RFFs of the emitter individuals, the SEI problem in a Rayleigh channel has been effectively solved. It is still not possible to establish an accurate mathematical model that explains the generation mechanism of RFFs. Therefore, deep learning techniques have been widely adopted to avoid expert intervention for SEI. Zhang et al. [17] have proposed a method of SEI using a convolutional neural network (CNN). In reference [18], seven ZigBee devices have been successfully identified, utilizing the error of the received baseband signal as the input of CNN. The long short-term memory (LSTM) technique has been adopted in reference [19] to learn the high-order correlation of received signals to identify multiple USRP devices effectively. In reference [20], transient signals have been processed by recurrence plots (RP) transforms, continuous wavelet transforms, and short-time Fourier transforms, respectively, before being fed to the CNN.

Consequently, 12 wireless devices have been successfully identified. Wong et al. [21] proposed a CNN model devised to estimate the gain deviation and phase deviation of the in-phase and quadrature components of the RF signals to identify the emitter individuals. He and Wang [22] proposed three signal preprocessing schemes: empirical mode decomposition (EMD), intrinsic time-scale decomposition (ITD), and VMD. Subsequently, an LSTM network has been used to extract RFFs to perform SEI.

The existing methods have promoted the development of SEI technologies; however, these methods can only achieve good identification performance when there are sufficient training samples. In practice, SEI technologies are mainly used in noncooperative scenarios, where it is difficult to obtain many signal samples with labeled information. Therefore, the traditional deep learning models are incapable of obtaining good training results, resulting in limited identification performance of the system. In this study, an SEI method in the few-shot scenario was proposed.

First, a signal preprocessing method based on VMD and the Hilbert analysis was introduced, which transformed the original RF signal into a Hilbert time-frequency spectrum to highlight its RFFs and thus enhance the distinguishability of different types of RF signals. Next, the classification neural network model was built, with the Hilbert time-frequency spectrum as its training samples, and the meta-learning algorithm was employed to conduct the training. Subsequently, the proposed network's ability to uncover the intrinsic and general characteristics of the signal data under test with only a few training samples was verified. Therefore, the proposed method has good identification performance and can effectively solve the few-shot SEI problem.

The remainder of this paper is organized as follows. In Section 2, we introduce the signal preprocessing scheme based on variational mode decomposition and the Hilbert analysis. In Section 3, we introduce the proposed few-shot SEI method based on meta-learning. In Section 4, we present and discuss the experimental results. Finally, we conclude the paper.

2. Signal Preprocessing

2.1. Variational Mode Decomposition. As a new signal decomposition technique, VMD can decompose nonlinear signals in the time domain and frequency domain to obtain finite modal components [23], which can be realized by modeling the constrained variational problem as follows:

$$\min_{v_k,\omega_k}\left\{\sum_{k=1}^{K}\left\|\frac{\partial}{\partial t}\left[\left(\delta(t)+\frac{j}{\pi t}\right)\times v_k(t)\right]e^{-j\omega_k t}\right\|_2^2\right\} \quad \text{s.t.}\sum_{k=1}^{K}v_k(t)=f(t), \tag{1}$$

where $v_k(t)$ represents the k-th modal component, ω_k represents the corresponding central frequency, $f(t)$ represents the original signal, and $\delta(t)$ represents the impulse function.

The constrained variational problem can be solved by the augmented Lagrangian multiplier algorithm, where the augmented Lagrangian function $D(\{v_k(t)\},\{\omega_k\},\lambda(t))$ can be expressed as follows:

$$D(\{v_k(t)\},\{\omega_k\},\lambda(t))=\left(\sum_{k=1}^{K}\left\|\frac{\partial}{\partial t}\left[\left(\delta(t)+\frac{j}{\pi t}\right)\times v_k(t)\right]e^{-j\omega_k t}\right\|_2^2\right)+\left\|f(t)-\sum_{k=1}^{K}v_k(t)\right\|_2^2+\lambda(t)\left(f(t)-\sum_{k=1}^{K}v_k(t)\right), \tag{2}$$

where $\lambda(t)$ represents the Lagrange multiplier. The modal component $\{v_k(t)\}$ can be obtained by solving the saddle point according to the augmented Lagrangian function $D(\{v_k(t)\},\{\omega_k\},\lambda(t))$. The alternate direction method of multipliers (ADMM) algorithm was used to resolve the problem through the following sequence:

Step 1: update the modal component as follows:

$$V_k^{n+1}(\omega)=\frac{F(\omega)-\sum_{j\neq k}V_j^n(\omega)+\Lambda(\omega)/2}{1+2\alpha(\omega-\omega_k^n)^2} \tag{3}$$

Step 2: update the central frequency as follows:

$$\omega_k^{n+1} = \frac{\int_0^\infty \omega |V_k(\omega)|^2 d\omega}{\int_0^\infty |V_k(\omega)|^2 d\omega} \tag{4}$$

Step 3: update the Lagrange multiplier as follows:

$$\Lambda(\omega) = \Lambda(\omega) + \varsigma \left[F(\omega) - \sum_{k=1}^{K} V_k(\omega) \right] \tag{5}$$

Step 4: repeat Steps 1 to 3 until the following condition is achieved:

$$\sum_{k=1}^{K} \left\| V_k^{n+1}(\omega) - V_k^n(\omega) \right\|_2^2 < \varepsilon, \tag{6}$$

where $F(\omega)$ represents the spectrum of the original signal $f(t)$, $V_k(\omega)$ represents the spectrum of the modal component $v_k(t)$, $\Lambda(\omega)$ represents the spectrum of the Lagrange multiplier $\lambda(t)$, n represents the iterative variable, and ε represents the threshold coefficient (assuming $\varepsilon = 10^{-6}$ in this study).

2.2. Hilbert Analysis. First, the Hilbert transformation is applied [24] to the decomposed modal components as follows:

$$\hat{v}_k(t) = \frac{1}{\pi} \int_{-\infty}^{\infty} \frac{v_k(t)}{t - \tau} d\tau. \tag{7}$$

Consequently, the instantaneous amplitude $a_k(t)$ and instantaneous frequency $\omega_k(t)$ of each modal component are calculated as follows:

$$a_k(t) = \sqrt{v_k^2(t) + \hat{v}_k^2(t)}, \tag{8}$$

$$\theta_k(t) = \arctan \frac{\hat{v}_k(t)}{v_k(t)}, \tag{9}$$

$$\omega_k(t) = \frac{d\theta_k(t)}{dt}. \tag{10}$$

The Hilbert time-frequency spectrum of the signal after Hilbert transformation is as follows:

$$H(t, \omega) = \mathrm{Re} \left[\sum_{k=1}^{K} a_k(t) e^{j \int \omega_k(t) dt} \right]. \tag{11}$$

3. Few-Shot Specific Emitter Identification Method Based on Meta-Learning

3.1. Classification Neural Network Model. The classification neural network model [25] was used to process RF signals to extract RFFs comprehensively, and its structure is shown in Figure 1.

The Hilbert time-frequency spectrum of the original RF signal was used as the network input vector $\boldsymbol{x}$. First, it was fed into a CNN of multiple convolution layers (CNN I, II, and III) for feature extraction. The convolution layers contained several convolution kernels, which were used to convolute the feature map from the previous layer. The ReLU function was used to activate the convolution layers and introduce nonlinear factors, which was helpful in the extraction of complex deep features [26, 27]. Subsequently, vectorization of distributed features was realized using the extracted feature maps through the fully connected layers (Dense I and II). Finally, the output vector of the last fully connected layer Dense II was mapped by the softmax function to obtain C different output probabilities, among which the highest probability corresponded to the specific type of the identified emitting source.

The training loss function of the classification neural network model can be expressed as follows:

$$J(\boldsymbol{x}; \theta) = -\frac{1}{C} \sum_{i=1}^{C} \sum_{n=1}^{N} \boldsymbol{y}_i \times \log \left[f_\theta \left(\boldsymbol{x}_i^{(n)} \right) \right], \tag{12}$$

where $\boldsymbol{x}_i^{(n)}$ represents the n-th Hilbert time-frequency spectrum sample corresponding to RF signals of class i, $f_\theta(\cdot)$ represents the mapping function of the classification neural network model with weight parameter θ, and $\boldsymbol{y}_i$ represents the label vector of class i, which is represented by the single one-hot encoding vector.

3.2. Meta-Learning. Traditional machine learning algorithms required multiple signal samples with labels to train the classification neural network model introduced in the previous section. However, in practice, it is challenging to label multiple signal samples. Consequently, unfit training networks and unsatisfactory results were obtained. Therefore, the meta-learning [28] algorithm was proposed, which utilized only a small number of labeled signal samples for network training. Unlike traditional machine learning techniques, the basic training unit of meta-learning is a task [29], generated using the following procedure: (1) assume that the training data set D_{train} contains C classes of signals, and $C_1 (C_1 < C)$ classes of signals are randomly selected to form a training subdataset $D_{sub-train}$; (2) for each class that belongs to C_1, P training samples are randomly sampled to form a support set $S_m = \{(\boldsymbol{x}_{sm}, y_{sm})\}$, which contains a total of $C_1 \times P$ signal training samples; (3) a query set $Q_m = \{(\boldsymbol{x}_{qm}, y_{qm})\}$ is formed by sampling R training samples from the remaining data of each signal class, which contains a total of $C_1 \times R$ signal training samples; (4) finally, a task $T_m = (S_m, Q_m)$is formed by support set S_m and query set Q_m, and accordingly, the universal set of tasks $T = \{T_1, T_2, \cdots, T_m, \cdots, T_M\}$ is obtained for meta-learning.

For the task T_m, the parameter θ of the meta-learner is assigned to a temporary network, which has the same structure as the meta-learner, and its network parameter is defined as φ_m. Next, the temporary network is trained using a support set S_m, whose loss function can be expressed as follows:

$$L_{T_m}((\boldsymbol{x}_{sm}, y_{sm}); \theta) = -\frac{1}{C_1} \sum_{i=1}^{C_1} \sum_{n=1}^{P} \boldsymbol{y}_{sm,i} \times \log \left[f_\theta \left(\boldsymbol{x}_{sm,i}^{(n)} \right) \right]. \tag{13}$$

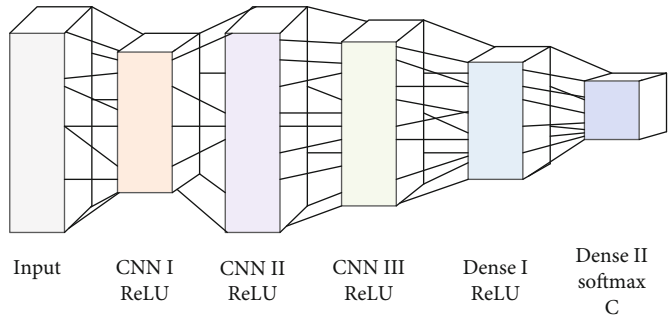

Figure 1: Structure of the classification neural network model.

Consequently, the parameter φ_m of the temporary network can be updated as follows:

$$\varphi_m = \theta - \alpha \cdot \frac{\partial L_{T_m}((\boldsymbol{x}_{sm}, y_{sm}); \theta)}{\partial \theta}, \tag{14}$$

where α represents the learning rate used to train the temporary network.

Subsequently, the temporary network is tested by query set Q_m, and the gradient loss is calculated to optimize the meta-learner's parameters as follows:

$$L_{T_m}\left(\left(\boldsymbol{x}_{qm}, y_{qm}\right); \varphi_m\right) = -\frac{1}{C_1}\sum_{i=1}^{C_1}\sum_{n=1}^{R} \boldsymbol{y}_{qm,i} \times \log\left[f_{\varphi_m}\left(\boldsymbol{x}_{qm,i}^{(n)}\right)\right], \tag{15}$$

$$\theta \longleftarrow \theta - \beta \times \nabla_{\varphi_m} \frac{\partial L_{T_m}\left(\left(\boldsymbol{x}_{qm}, y_{qm}\right); \varphi_m\right)}{\partial \varphi_m}, \tag{16}$$

where β represents the learning rate used to train the meta-learner.

It is discernible that the temporary network focuses on exploring the characteristics of a single task through data analysis and modeling, while the meta-learner specializes in understanding the common feature representation of all tasks through summarizing and analyzing the training results of the temporary network. Specifically, the common feature representation of the tasks represents the general and intrinsic characteristics implied in the training data. A good understanding of such common characteristics acquired by the meta-learner indicates its promising capability for generalization. Accordingly, the meta-learner can provide more optimal initial values to the temporary network on the new tasks, thus making the temporary network achieve training fitting through a few iterations on the condition of few samples. The training results are fed back to the meta-learner to improve its generalization performance further [30]. Therefore, the meta-learning algorithm is considered suitable for few-shot training.

3.3. Algorithm Flow. Based on the theoretical analyses presented in previous sections, the algorithm flow of specific emitter identification based on meta-learning is summarized in this section.

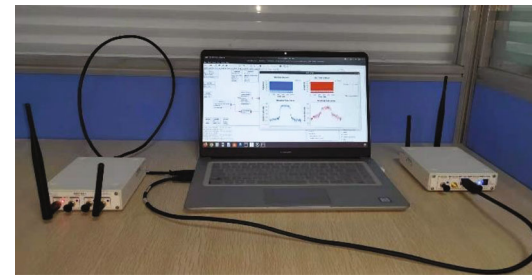

Figure 2: SDR platform.

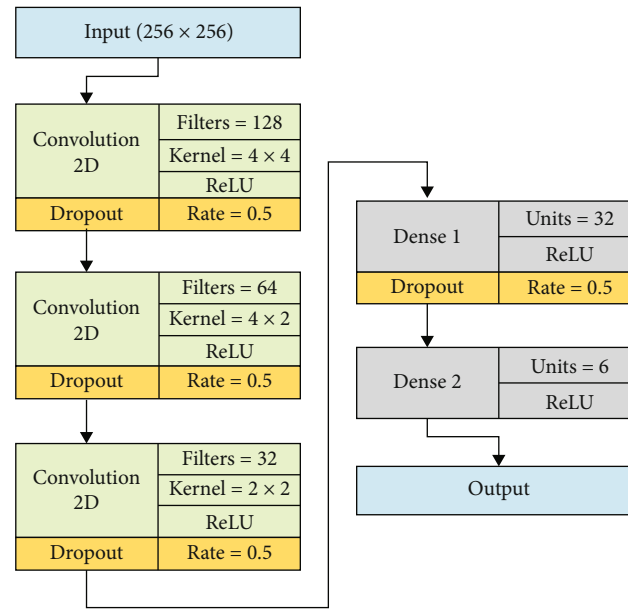

Figure 3: Structure of the classification neural network model.

Step 1: obtain the Hilbert time-frequency spectrum through preprocessing the received RF signals, which is used as the training sample to construct the training data set D_{train} that contains C classes of signals.

Step 2: acquire M meta-learning tasks $T = \{T_1, T_2, \cdots, T_m, \cdots, T_M\}$ by sampling the training data set D_{train}.

Step 3: for task T_m, train the temporary network with support set S_m according to Equation (13); and then update the temporary network parameter φ_m following Equation (14).

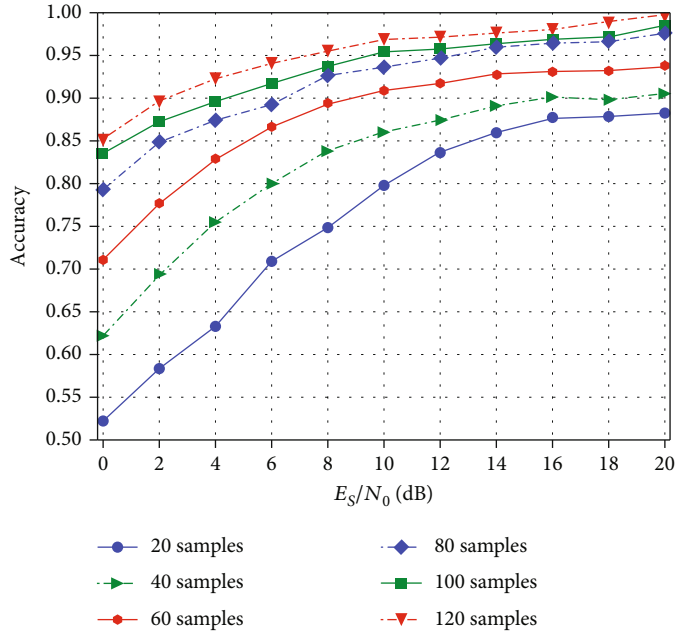

Figure 4: Identification accuracy on different numbers of training samples.

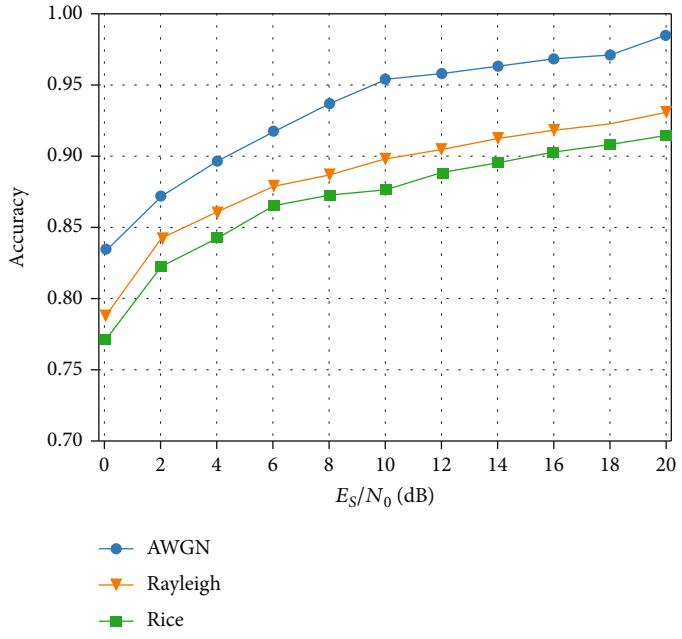

Figure 5: Identification accuracy of different propagation channels.

Step 4: test the temporary network with query set Q_m; calculate the gradient loss based on Equation (15); and then optimize the meta-learner parameters according to Equation (16).

Step 5: repeat Steps 3 and 4 until meta-learning of all tasks is completed.

4. Experiment Results and Analyses

4.1. Data Acquisition and Network Modeling. This section explains the experiments' data acquisition through a software-defined radio (SDR) platform, as shown in Figure 2.

Seven USRP devices of the same model were used to obtain signals from different emitter individuals, with six working as radio emitters and one working as the radio receiver. Each side was connected to a PC, defining either the transmitting or receiving behavior through a GNU radio. The receiver captured six different types of RF signals emitted from the defined emitters. The working frequency of the transmitted signal was set to 2.4 GHz, and the sampling frequency at the receiver end was 16 MHz. QPSK modulation was applied to all the six emitters with a bandwidth of 1.2 MHz. Each received signal was divided to record 1000 units of data, each with 256 sampling points.

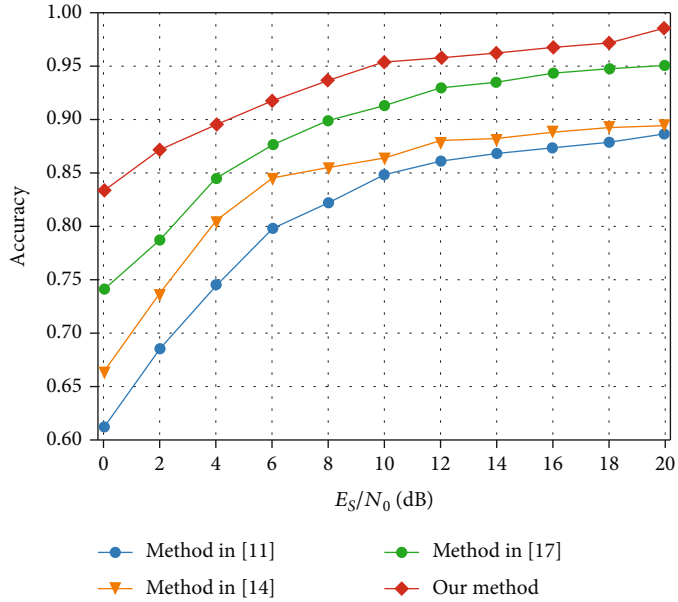

Figure 6: Identification accuracy of different methods.

Signal transmission and capture were carried out in a laboratory environment to ensure a high data quality. It is necessary to test the identification performance under different signal-to-noise (SNR) conditions by artificially adding noises to the signal to verify the algorithm's robustness to noises. The originally captured signal data was sent to MATLAB for the additional noises in the experiments, with the SNR set to 0, 2,…, 20 dB.

The neural network model—comprising the input layer, CNN layers, fully connected layers, and the softmax classification activation function—was built based on the structure presented in Figure 1. The structure of the classification neural network model is shown in Figure 3.

4.2. Impact of the Number of Training Samples on Identification Performance. This section focuses on the impact of the number of training samples on identification performance. We train CNN through meta-learning, where the number of labelled training samples is set to 20, 40, 60, 80, 100, and 120. We then test the identification accuracy under different SNRs, and the identification accuracy curve is shown in Figure 4.

As shown in Figure 4, as the number of labelled samples increases, the overall identification accuracy also increases. However, when the number of training signal samples reaches 80, the identification performance of the system is stable and maintains a high level, indicating that the proposed method can well adapt to the few-shot specific emitter identification task. Therefore, with only a few labelled signal samples for training, the system can exhibit satisfactory identification performances.

4.3. Robustness to Noise. As RFFs are subtle and vulnerable to noise interference during wireless channel transmission, the robustness of the proposed method to noise is crucial to its identification performance. This section prepared different propagation channels with additive white Gaussian noise (AWGN), Rayleigh noise, and Rice noise added to the signal data, respectively. The identification accuracy of each channel under different SNRs was obtained and plotted in Figure 5.

As shown in Figure 5, the best identification performance is achieved in the AWGN channel, with an identification accuracy of 90% at 4 dB and more than 95% at 10 dB. In contrast, the identification performances were poorer in both Rayleigh and Rice channels because the noises in Rayleigh and Rice channels are multiplicative noises, which have a more significant impact on RFFs extraction than the additive noises in AWGN channels. However, under the interference of multiplicative noises, the system's identification accuracy did not deteriorate further. For the Rayleigh channel, an accuracy of 85% at 4 dB and 90% at 10 dB was observed. For the Rice channel, the accuracy at 4 dB and 14 dB was 85% and 90%, respectively. The experimental results implied that the proposed method was robust to noises of different wireless transmission channels.

4.4. Other Indices to Evaluate the Identification Performance. The identification accuracy is defined as the ratio of the number of correctly classified samples to the total number of samples under test, which can only evaluate the identification performance of the system as a whole rather than the identification performance of each type of signal. In this section, the receiver operating characteristic (ROC) was used as an index to further evaluate the identification performance of the proposed method, as shown in Figure 6, with the SNR set to 6, 12, and 20 dB, respectively.

As shown in Figure 7, all the ROC curves of the proposed method are generally distributed in the upper left region of the plot—the higher the SNR, the more concentrated the ROC curve is within the region. Both the high true-positive rate and a low false-positive rate achieved for identifying each USRP device show the suggested method's promising performance in the area of SEI. In addition, the

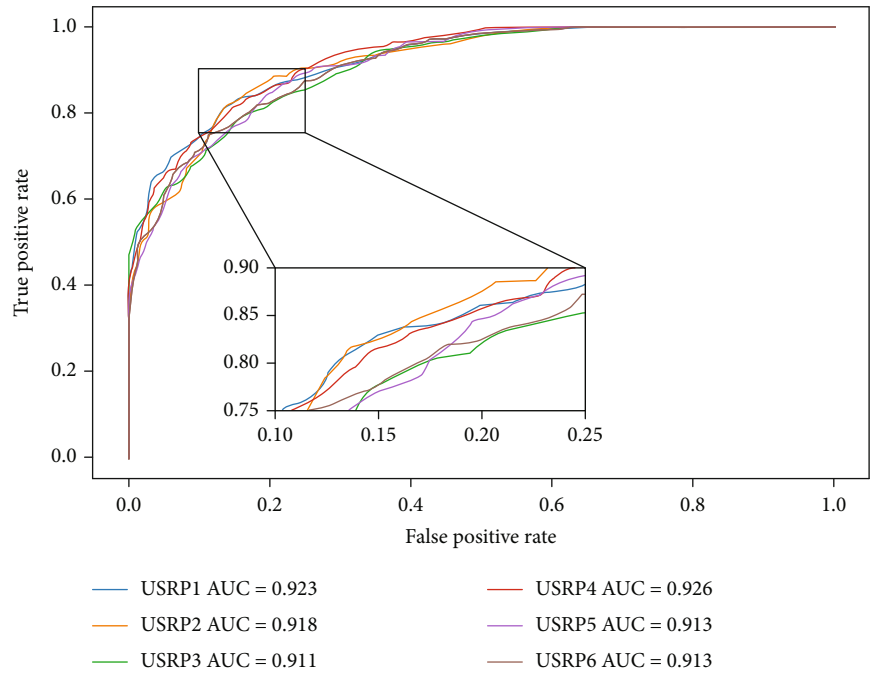

(a)

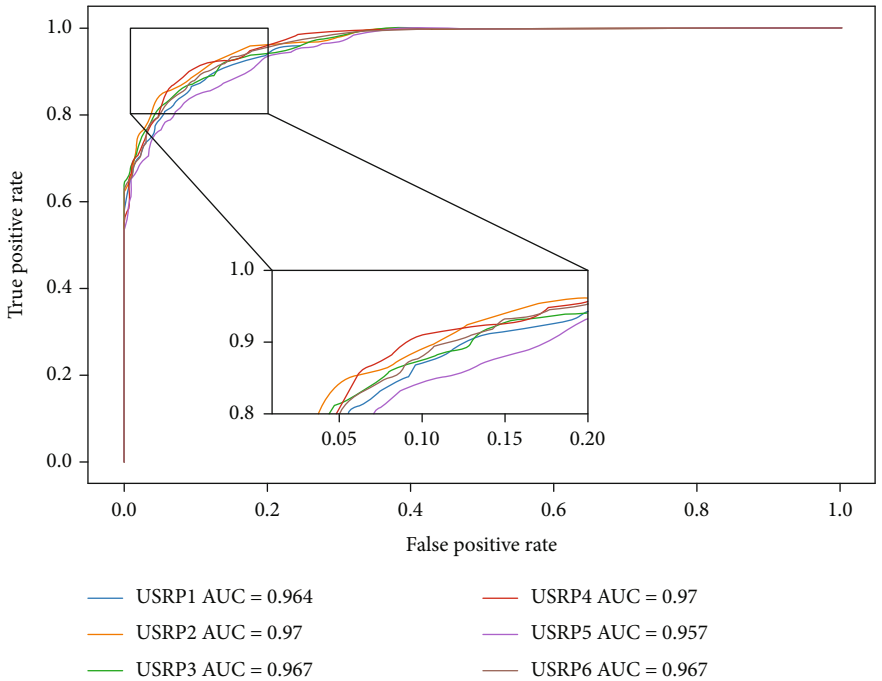

(b)

Figure 7: Continued.

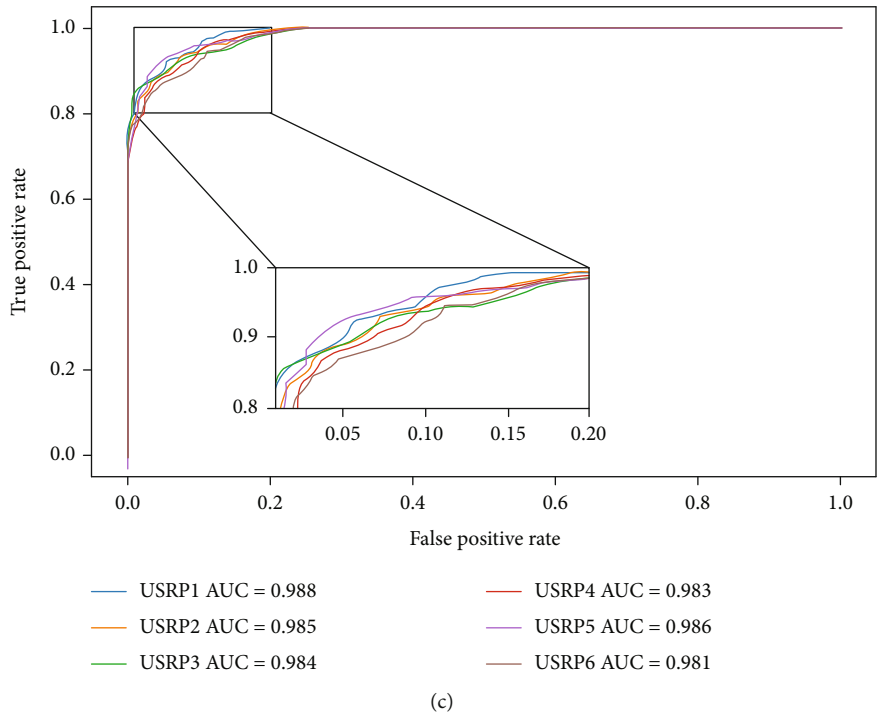

(c)

Figure 7: ROC curves of the proposed method at 6 dB, 12 dB, and 20 dB, respectively. (a) SNR = 6 dB. (b) SNR = 12 dB. (c) SNR = 20 dB.

area under the curve (AUC) was calculated. In Figure 6, the AUC value of each ROC curve is greater than 0.91 at 6 dB, greater than 0.95 at 12 dB, and greater than 0.98 at 20 dB, further proving the good identification performance of the proposed method quantitatively.

4.5. Comparison with Other Identification Methods. The above experiments proved the effectiveness and efficiency of the proposed method in SEI for a few-shot scenario. This section benchmarks the study with those proposed in references [11, 14, 17] to examine its advantages. The experimental results of the methods mentioned above are shown in Figure 6.

As shown in Figure 6, the identification accuracy of this method is higher than that of other methods in each defined SNR scenario, and the overall identification accuracy is 5–15% higher than the other methods. In addition, in a low SNR scenario, the proposed method can still achieve an identification accuracy above 0.8, whereas all the other methods showed deteriorated performances. The proposed method outperforms the experiments due to its adoption of meta-learning, which can thoroughly learn the general and intrinsic characteristics of the signals. On the contrary, the methods for benchmarking rely on a large quantity of samples to train the neural networks and establish simple mapping relationships between signal data and classes. When the number of training samples is reduced, the generalization ability of these networks is degraded, and their identification performances are affected.

5. Conclusion

In this study, a method of few-shot specific emitter identification is proposed. First, the received RF signal was preprocessed based on VMD. Next, the Hilbert time-frequency spectrum was obtained through the Hilbert analysis of the modal components. Such spectrums were used as the training samples of the classification neural network to carry out meta-learning to ensure that the neural network achieves good training results with a limited number of training samples. The experimental results showed that this method could achieve excellent identification performance and strong robustness to noise with only 80 training samples. Finally, the proposed method demonstrated better identification performances than other existing methods because it can effectively solve SEI problems in the few-shot scenario.

In future work, focus will be on identifying specific emitters in open-set few-shot scenarios. In other words, the method used to detect open-set RF signals while normally identifying different types of closed-set RF signals will be investigated based on the results of this study. In addition, real-world RF signals were captured for experimental verifications to justify further and improve the versatility of the proposed method.

Data Availability

The data used to support the findings of this study are available from the corresponding author upon request.

Conflicts of Interest

The authors declare no conflicts of interest.

Acknowledgments

This work was supported in part by the National Natural Science Foundation of China under grant 91538201, in part by the Taishan Scholar Project of Shandong Province under grant

ts201511020, and in part by the Project supported by Chinese National Key Laboratory of Science and Technology on Information System Security under grant 6142111190404.

References

[1] L. Li, H.-B. Ji, and L. Jiang, "Quadratic time–frequency analysis and sequential recognition for specific emitter identification," *IET Signal Process*, vol. 5, no. 6, pp. 133–568, 2011.

[2] S. Rajendran, Z. Sun, F. Lin, and K. Ren, "Injecting reliable radio frequency fingerprints using metasurface for the internet of things," *IEEE Transactions on Information Forensics and Security*, vol. 32, no. 1, pp. 27–33, 2007.

[3] K. Sa, D. Lang, C. Wang, and Y. Bai, "Specific emitter identification techniques for the internet of things," *IEEE Access*, vol. 8, pp. 1644–1652, 2020.

[4] K. I. Talbot, P. R. Duley, and M. H. Hyatt, "Specific emitter identification and verification," *Technology Review Journal*, vol. 113, pp. 130–133, 2003.

[5] A. E. Spezio, "Electronic warfare systems," *IEEE Transactions on Microwave Theory and Techniques*, vol. 50, no. 3, pp. 633–644, 2002.

[6] M. Liu and J. F. Doherty, "Nonlinearity estimation for specific emitter identification in multipath channels," *IEEE Transactions on Information Forensics and Security*, vol. 6, no. 3, pp. 1076–1085, 2011.

[7] S. Haykin, "Cognitive radio: brain-empowered wireless communications," *IEEE Journal on Selected Areas in Communications*, vol. 23, no. 2, pp. 201–220, 2005.

[8] S. Khoshabi Nobar, K. Adli Mehr, and J. Musevi Niya, "RF-powered green cognitive radio networks: architecture and performance analysis," *IEEE Communications Letters*, vol. 20, no. 2, pp. 296–299, 2016.

[9] A. Ghosh and W. Hamouda, "Cross-layer antenna selection and channel allocation for MIMO cognitive radios," *IEEE Transactions on Wireless Communications*, vol. 10, no. 11, pp. 3666–3674, 2011.

[10] V. Shakhov and I. Koo, "Analysis of a network stability-aware clustering protocol for cognitive radio sensor networks," *IEEE Internet of Things Journal*, vol. 8, no. 15, pp. 12476-12477, 2021.

[11] O. B. Akan, O. B. Karli, and O. Ergul, "Cognitive radio sensor networks," *IEEE Network*, vol. 23, no. 4, pp. 34–40, 2009.

[12] M. Zheng, C. Wang, M. Du, L. Chen, W. Liang, and H. Yu, "A short preamble cognitive MAC protocol in cognitive radio sensor networks," *IEEE Sensors Journal*, vol. 19, no. 15, pp. 6530–6538, 2019.

[13] P. Padilla, J. L. Padilla, and J. F. Valenzuela-Valdés, "Radiofrequency identification of wireless devices based on RF fingerprinting," *Electronics Letters*, vol. 49, no. 22, pp. 1409-1410, 2013.

[14] Y. J. Yuan, Z. T. Huang, H. Wu, and X. Wang, "Specific emitter identification based on Hilbert–Huang transform-based time–frequency–energy distribution features," *IET Communications*, vol. 8, no. 13, pp. 2404–2412, 2014.

[15] J. Zhang, F. Wang, O. A. Dober, and Z. Zhong, "Specific emitter identification via Hilbert-Huang transform in single-hop and relaying scenarios," *IEEE Transactions on Information Forensics and Security*, vol. 11, no. 6, pp. 1192–1205, 2016.

[16] U. Satija, N. Trivedi, G. Biswal, and B. Ramkumar, "Specific emitter identification based on variational mode decomposition and spectral features in single hop and relaying scenarios," *IEEE Transactions on Information Forensics and Security*, vol. 14, no. 3, pp. 581–591, 2019.

[17] M. Zhang, M. Diao, and L. Guo, "Convolutional neural networks for automatic cognitive radio waveform recognition," *IEEE Access*, vol. 5, pp. 11074–11082, 2017.

[18] K. Merchant, S. Revay, G. Stantchev, and B. Nousain, "Deep learning for RF device fingerprinting in cognitive communication networks," *IEEE Journal of Selected Topics in Signal Processing*, vol. 12, no. 1, pp. 160–167, 2018.

[19] Q. Wu, C. Feres, D. Kuzmenko et al., "Deep learning based RF fingerprinting for device identification and wireless security," *Electronics Letters*, vol. 54, no. 24, pp. 1405–1407, 2018.

[20] G. Baldini, C. Gentile, R. Giuliani, and G. Steri, "Comparison of techniques for radiometric identification based on deep convolutional neural networks," *Electronics Letters*, vol. 55, no. 2, pp. 90–92, 2019.

[21] L. J. Wong, W. C. Headley, and A. J. Michaels, "Specific emitter identification using convolutional neural network-based IQ imbalance estimators," *IEEE Access*, vol. 7, pp. 33544–33555, 2019.

[22] B. X. He and F. G. Wang, "Cooperative specific emitter identification via multiple distorted receivers," *IEEE Transactions on Information Forensics and Security*, vol. 15, pp. 3791–3806, 2020.

[23] K. Dragomiretskiy and D. Zosso, "Variational mode decomposition," *IEEE Transactions on Signal Processing*, vol. 62, no. 3, pp. 531–544, 2014.

[24] H. Li, D. Xiao, S. Kwong, L. Yang, D. Huang, and D. Xiao, "Hilbert-Huang transform for analysis of heart rate variability in cardiac health," *IEEE/ACM Transactions on Computational Biology and Bioinformatics*, vol. 8, no. 6, pp. 1557–1567, 2011.

[25] Y. Lecun, Y. Bengio, and G. Hinton, "Deep learning," *Nature*, vol. 521, no. 7553, pp. 436–444, 2015.

[26] L. Han, J. Z. Sun, and W. Zhang, "Convolutional neural network for convective storm nowcasting using 3-D doppler weather radar data," *IEEE Transactions on Geoscience and Remote Sensing*, vol. 58, no. 2, pp. 1487–1495, 2019.

[27] T. O'Shea and J. Hoydis, "An introduction to deep learning for the physical layer," *IEEE Transactions on Cognitive Communications and Networking*, vol. 3, no. 4, pp. 563–575, 2017.

[28] C. Finn, P. Abbeel, and S. Levine, "Model-agnostic meta-learning for fast adaptation of deep networks," *In Proceeding of the 34th International Conference on Machine Learning*, vol. 70, pp. 1126–1135, 2017.

[29] M. Andrychowicz, M. Denil, S. Gomez et al., "Learning to learn by gradient descent by gradient descent," *Advances in Neural Information Processing Systems*, vol. 29, pp. 3981–3989, 2016.

[30] T. Y. Mu, H. Z. Wang, C. N. Wang, Z. Liang, and X. Shao, "Auto-CASH: a meta-learning embedding approach for autonomous classification algorithm selection," *Information Sciences*, vol. 591, pp. 344–364, 2022.